

# Automatic Analysis of Fetal Echographic Images

Sandra Vilas Boas Jardim\*, Mário A. T. Figueiredo\*\*

\*Escola Superior de Tecnologia - Instituto Politécnico de Castelo Branco  
6000-767 Castelo Branco, Portugal

\*\*Instituto de Telecomunicações, Instituto Superior Técnico  
1049-001 Lisboa, Portugal

**Abstract** – This paper describes a new method for the automatic extraction and measurement of fetal anatomic structures from echographic images. More specifically, we estimate and measure the contours of the femur and of cranial cross-sections of fetal bodies. Contour estimation is formulated as a statistical estimation problem, where both the contour and the observation model parameters are unknown. The observation model (or likelihood function) relates, in probabilistic terms, the observed image with the underlying contour. This likelihood function is derived from a region-based image model. The contour and the parameters are estimated according to the *maximum likelihood* (ML) criterion, via unsupervised deterministic iterative algorithms. Experiments reported in the paper, using synthetic and real images, testify for the adequacy and good performance of the proposed approach.

**Keywords** – Ultrasound images, contour estimation, deformable models, maximum likelihood, region-based image model, image segmentation.

## I. INTRODUCTION

Ultrasound imaging (echography) is a very important medical diagnostic auxiliary tool. Its relatively low cost, short acquisition time, and non invasive nature makes echography a very competitive modality. This fact has stimulated a great amount of research aimed at increasing its diagnostic potential [1].

Measurements based on echographic images play a significant role in obstetrics as an accurate means for fetal age estimation. Several parameters are used as age and development indicators, the most important of which are: *biparietal diameter* (BPD), *occipital-frontal diameter* (OFD), *head circumference* (HC), and *femur length* (FL) [2]. Each of these parameters provides, through a specific mathematical expression, estimates of the gestational age (GA), given in weeks (w) and days (d) [2]. Consistency and reliability of measurements is thus a very important issue.

Manual extraction of contours in medical images requires expert knowledge and is a tedious and time-consuming task. In addition, manual contour extraction is influenced by the variability of the human observer which limits its reliability and reproducibility. The development of automatic techniques for the extraction of contours of fetal anatomic structures can in principle eliminate the variability intro-

duced by the human operator, contributing to reliable and reproducible measurements. In the development of such techniques, important factors determining its acceptance by clinicians are: accuracy, robustness, reliability, reproducibility, and applicability.

While a great deal of research has been published on automated contour estimation in cardiological and brain imaging, the same does not seem to be true for obstetric ultrasound imaging. The only publications known to the authors on this topic are [3] and [4].

The formation process of an ultrasound image involves different types of random perturbations, such as the displaying of non-structural echoes, removal of real structural echoes, displacement and distortion of echoes, and distortion of the organ dynamics [5]. To these types of artifacts we must add the speckle noise, considered the most important perturbation in ultrasound images. This type of noise is Rayleigh multiplicative and degrades the image by hiding thin structures and reducing the signal-to-noise ratio (SNR) [6]. The presence of these perturbation makes conventional techniques for contour extraction in digital images (such as those based on local estimates of the image gradient) inappropriate for contour extraction in ultrasound images [7]. More generally, any segmentation algorithm that is sensitive to noise is not useful for segmenting ultrasound images.

In this paper, we describe a new method for the automatic estimation of contours of the femur and of cranial cross-sections, which is an indispensable first step towards an automatic measurement system. To deal with the low quality of echographic images, which makes any contour detection task very difficult, we use low order parameterizations of the contour shapes. This low-order parameterization is sufficient to accommodate the expected shape and size variations of the organs, but provides robustness against noise, image artifacts, and regions of missing data. The problem is formulated in a statistical estimation framework, and implementation is carried out by unsupervised deterministic iterative algorithms.

## II. ACTIVE AND DEFORMABLE CONTOURS

Snakes, or active contour models [8], and their conceptual descendants, have been often adopted to deal with contour/boundary estimation problems in several application

contexts. A relevant example is medical imaging, where contour estimation is the fundamental first step of many automatic image analysis systems [7, 9]. Active contour models are controlled by a number of different (virtual) forces acting simultaneously, where each force results from the minimization of a separate term of a so-called *energy function*. Usually, these terms include an *internal* energy, which is responsible for keeping the model smooth, and an *external* energy which attracts the model towards the image features of interest. During the application of an active contour model to an image, these forces compete until an equilibrium configuration is reached, in which the global energy is minimized. Several drawbacks of conventional snakes, such as the strict use of local data, have stimulated a great amount of research [10], [11], [12], [13], [14]. Although most limitations of the original formulation have been successfully addressed, only special-purpose approaches have been able to deal with ultrasound images [7].

Active contour models (or their probabilistic reformulations [7, 12, 15]) require careful tuning of several involved parameters, such as those controlling the trade-off between smoothness/robustness and estimation accuracy. This fact limits the use of these methods for practical medical imaging applications. Moreover, the quality of fetal ultrasound images is often so low that a simple smoothness term is not sufficient to ensure adequate contour estimates.

Deformable models constitute another important approach to contour estimation. Here, global models generally described by a small number of parameters are used (in contrast with snakes, which typically use explicit contour descriptions). The model parameters are then estimated in the presence of the observed image. Deformable models usually do not include a smoothness energy term since the simplicity of the parameterization itself guarantees regularity and smoothness of the represented shape. Seminal work on deformable models was done by Grenander [16]; see also [17], [18], [19], [20], and other references therein.

### III. PROPOSED APPROACH: MAXIMUM LIKELIHOOD PARAMETRIC DEFORMABLE MODELS

#### A. Statistical Estimation

As mentioned above, we will formulate contour estimation by adopting a maximum likelihood criterion. To specify this criterion, we need to consider:

- the observed data set  $\mathbf{Z}$ , which in our case is the set of all image pixels;
- a probabilistic model indexed by the parameter vector  $\theta$ , that is  $p(\mathbf{Z}|\theta)$ , where  $\theta$  is a set of parameters describing the contour shape.

Under the maximum likelihood criterion, the best estimate of  $\theta$ , denoted  $\hat{\theta}_{\text{ML}}$ , is given by

$$\hat{\theta}_{\text{ML}} = \arg \max_{\theta} p(\mathbf{Z}|\theta). \quad (1)$$

To derive the likelihood function  $p(\mathbf{Z}|\theta)$ , we adopt a region-based model [7, 9, 12, 14, 15], which is an approach known to be robust with respect to local artifacts and poor image

quality. Region-based models are based on spatial characteristics of homogeneity, where the term homogeneity does not necessarily mean that the pixels in a given region have identical intensities, but that the differences inside a region are much less than between regions. The advantage of these models is that they directly depend on all the image data, being less sensitive to noise and image artifacts than methods that use derived information. Moreover, region-based models allow, in general, an easy derivation of the likelihood function, a main ingredient of any probabilistic formulation.

#### B. Observation model

The observed image  $\mathbf{Z}$  (a  $w_x \times w_y$  array of gray levels), is modelled as a random function of the object's boundary  $\mathbf{v}$ , which is a parametric function of unknown parameters, that is we write  $\mathbf{v}(\theta)$ . The likelihood function  $p(\mathbf{Z}|\theta, \phi)$  defines, in probabilistic terms, the image observation model, where the image plays the role of observed data, and  $\phi$  is a set of additional unknown parameters which characterize the observation model.

We adopt the simplest region-based model characterized by the two following hypotheses:

- **Conditional independence**

Given the contour, the image pixels are independently distributed;

- **Region homogeneity**

The conditional probability function of each pixel depends only on whether it belongs to the inside or outside region of the contour; i.e., all pixels inside (resp. outside) have a common distribution characterized by a parameter vector  $\phi_{\text{in}}$  (resp.  $\phi_{\text{out}}$ ), with  $\phi = [\phi_{\text{in}} \ \phi_{\text{out}}]$ .

Thus, the joint probability density function of the observed image, given a contour  $\mathbf{v}(\theta)$ , can be written as

$$p(\mathbf{Z}|\theta, \phi) = \prod_{(i,j) \in I(\mathbf{v}(\theta))} p(Z_{(i,j)}|\phi_{\text{in}}) \prod_{(i,j) \in O(\mathbf{v}(\theta))} p(Z_{(i,j)}|\phi_{\text{out}}), \quad (2)$$

with  $Z_{(i,j)}$  denoting the value of pixel  $(i, j)$ , while  $I(\mathbf{v}(\theta))$  and  $O(\mathbf{v}(\theta))$  are, respectively, the inside and outside regions of the contour  $\mathbf{v}(\theta)$ . Finally,  $p(Z_{(i,j)}|\phi_{\text{in}})$  and  $p(Z_{(i,j)}|\phi_{\text{out}})$  are, respectively, the pixel-wise probability functions, of the inner and outer regions.

Given that ultrasound images follow a Rayleigh distribution, the pixel-wise probability densities have the form

$$p(x|\sigma) = \frac{x}{\sigma} \exp\left\{-\frac{x^2}{2\sigma}\right\}, \quad \text{for } x \geq 0, \quad (3)$$

and thus  $\phi = [\sigma_{\text{in}} \ \sigma_{\text{out}}]$ , where  $\sigma_{\text{in}}$  and  $\sigma_{\text{out}}$  are the variances for the inside and outside regions, respectively.

#### C. Complete estimation criterion and algorithm

To implement an unsupervised scheme we must estimate, from an observed image  $\mathbf{Z}$ , not only the parameters that define the contour,  $\theta$ , but also the other parameters of the observation model,  $\phi$ . Accordingly, we extend the maximum

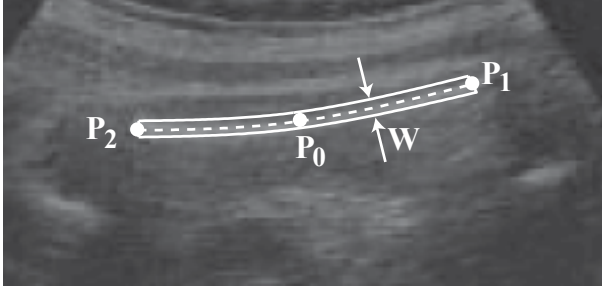


Figure 1 - Parameterization of the femur shape: the axis is a 3 point interpolating spline; the inside region is  $W$  pixels wide around the axis.

likelihood criterion to include also those parameters:

$$\left(\hat{\theta}, \hat{\phi}\right) = \arg \max_{\theta, \phi} \{\log p(\mathbf{Z}|\theta, \phi)\}, \quad (4)$$

where the log function is included because it does not affect the location of the maximum and allows some formal simplification. Since solving (4) simultaneously with respect to  $\theta$  and  $\phi$  would be computationally very difficult, we settle for a suboptimal solution given by iterative schemes of the type

$$\hat{\theta}^{(t+1)} = \arg \max_{\theta} \left\{ \log p(\mathbf{Z}|\theta, \hat{\phi}^{(t)}) \right\} \quad (5)$$

$$\hat{\phi}^{(t+1)} = \arg \max_{\phi} \left\{ \log p(\mathbf{Z}|\hat{\theta}^{(t+1)}, \phi) \right\}, \quad (6)$$

where  $\hat{\theta}^{(t)}$  and  $\hat{\phi}^{(t)}$  are the estimates of  $\theta$  and  $\phi$  at iteration  $t$ , respectively.

#### IV. IMPLEMENTATION

We have implemented two contour estimation algorithms: one for the fetal femur, and another for the fetal head. In both cases, the underlying criterion and type of algorithm are those in Equations (4), (5), and (6), although the parameterization of the contour shapes is naturally different.

The algorithm defined by Equations (5) and (6) can be seen as a 2-levels hierarchical scheme of nested algorithms: the inner scheme (**Algorithm 2**) updates  $\theta$  (Equation (5)), taking  $\phi$  fixed. **Algorithm 2** is then used by the global algorithm, termed **Algorithm 1**, to solve for both  $\theta$  and  $\phi$ .

##### A. Femur contour estimation algorithm

Given the form of a fetal femur (usually a straight line segment for a younger fetus, and a slightly curved arc for an older fetus [2]), we adopt an interpolating spline defined by only three points  $\theta = [P_0, P_1, P_2]$ . As shown in Figure 1, the inside region  $I(\mathbf{v}(\theta))$  is  $W$  pixels wide around the spline (dashed line). Although this is a very simple parameterization, it reveals itself rich enough to cover all the possible shapes of fetus femurs.

##### Algorithm 1

**Inputs:** An initial valid point  $\hat{P}_0^{\text{init}}$ . This point is given by the user who is asked to indicate a point somewhere inside the femur.

**Outputs:** The estimates  $\hat{\theta}^{\text{final}}$  and  $\hat{\phi}^{\text{final}}$ .

**Step 0:** Set  $t = 0$  (iteration counter). Set  $\hat{P}_0^{(t)} = \hat{P}_0^{\text{init}}$ . To set  $W$  and initialize  $\hat{P}_1^{(t)}$  and  $\hat{P}_2^{(t)}$  we use the following procedure: a straight line segment is defined such that  $\hat{P}_1^{(t)}$  and  $\hat{P}_2^{(t)}$  are the endpoints and  $\hat{P}_0^{(t)}$  is the midpoint. The angle of this line segment and the region width  $W$  are chosen by maximizing the variance measured in the corresponding inside region, while keeping  $\hat{P}_0^{(t)}$  fixed.

**Step 1:** Given the current contour  $\mathbf{v}(\hat{\theta}^{(t)})$ , update the estimates of the variance parameter  $\phi = [\sigma_{\text{in}} \ \sigma_{\text{out}}]$  according to the ML criterion,

$$\begin{aligned} \hat{\sigma}_{\text{in}}^{(t+1)} &= \arg \max_{\sigma_{\text{in}}} \log p(\mathbf{Z}|\hat{\theta}^{(t)}, [\sigma_{\text{in}} \ \sigma_{\text{out}}]) \\ &= \frac{1}{2|I^{(t)}|} \sum_{(i,j) \in I^{(t)}} Z_{(i,j)}^2. \end{aligned} \quad (7)$$

where  $I^{(t)} = I(\mathbf{v}(\hat{\theta}^{(t)}))$  is the current inside region, and  $|I^{(t)}|$  denotes the number of pixels in  $I^{(t)}$ ; a similar expression is used for  $\hat{\sigma}_{\text{out}}^{(t+1)}$ .

**Step 2:** Run **Algorithm 2**, providing  $\hat{\theta}^{(t)}$  and  $\hat{\phi}^{(t+1)}$  as inputs. **Algorithm 2** returns an updated  $\hat{\theta}^{(t+1)}$ .

**Step 3:** If some stopping criterion is met, terminate with outputs  $\hat{\theta}^{\text{final}} = \hat{\theta}^{(t+1)}$  and  $\hat{\phi}^{\text{final}} = \hat{\phi}^{(t+1)}$ ; otherwise, increment  $t$  and return to **Step 1**.

##### Algorithm 2

**Inputs:** A given parameter estimate  $\hat{\phi}$  and an initial contour parameter  $\hat{\theta}^{\text{first}}$ .

**Outputs:** An updated contour parameter estimate  $\hat{\theta}^{\text{new}}$ .

**Step 0:** Set  $q = 0$  (iteration counter). Set  $\hat{\theta}^{(q)} = \hat{\theta}^{\text{first}}$ .

**Step 1:** Update the contour parameters according to

$$\begin{aligned} \hat{P}_0^{(q+1)} &= \arg \max_{P_0 \in \mathcal{N}(\hat{P}_0^{(q)})} \log p(\mathbf{Z} | [P_0, \hat{P}_1^{(q)}, \hat{P}_2^{(q)}], \hat{\phi}), \\ \hat{P}_1^{(q+1)} &= \arg \max_{P_1 \in \mathcal{N}(\hat{P}_1^{(q)})} \log p(\mathbf{Z} | [\hat{P}_0^{(q)}, P_1, \hat{P}_2^{(q)}], \hat{\phi}), \\ \hat{P}_2^{(q+1)} &= \arg \max_{P_2 \in \mathcal{N}(\hat{P}_2^{(q)})} \log p(\mathbf{Z} | [\hat{P}_0^{(q)}, \hat{P}_1^{(q)}, P_2], \hat{\phi}), \end{aligned}$$

where  $\mathcal{N}(\hat{P}_i^{(q)})$  is the set of 8 nearest neighbors of  $\hat{P}_i^{(q)}$ , for  $i = 0, 1, 2$ .

**Step 2:** If a stopping criterion is met, output  $\hat{\theta}^{\text{new}} = \hat{\theta}^{(q+1)}$ ; if not, increment  $q$  and go back to **Step 1**.

##### B. Head contour estimation

The fetal head is approximately elliptical. In order to get a precise adjustment, we have parameterized the contour as an closed 8-point interpolating spline, that is,  $\theta = [P_1, \dots, P_8]$ . As illustrated in Figure 2, the inside region  $I(\mathbf{v}(\theta))$  is  $W$  pixels wide around the spline (dashed line).

To estimate the cranial cross-section, we use the same basic approach as described above for the femur. However, this turns out to be more difficult, mainly due to the presence of several intracranial structures which can wrongly

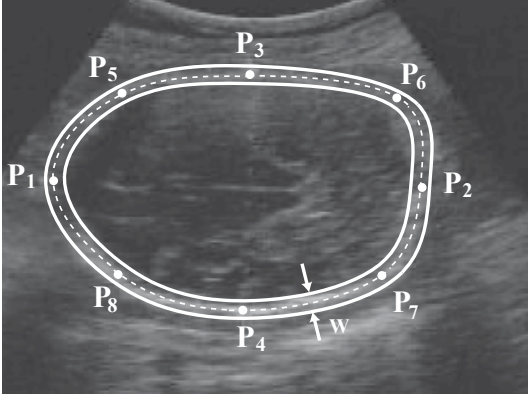


Figure 2 - Parameterization of the cranial cross-section wall.

attract the contour estimate. To avoid these intracranial artifacts, we add to the log-likelihood function a new term which forces the contour to move beyond undesired high variance regions. This approach, proposed in [11], is named *balloon*, since it makes the contour behave like an inflating balloon. The modified estimation criterion is thus

$$\left(\hat{\theta}, \hat{\phi}\right) = \arg \max_{\theta, \phi} \{\log p(\mathbf{Z}|\theta, \phi) + \lambda b(\theta)\}, \quad (8)$$

where  $b(\theta)$  is the *balloon* term, an increasing function of the contour area; here, we set  $b(\theta)$  to the area of the inscribing rectangle. The weight  $\lambda$  of this new term must be sufficient to allow the contour to move past the undesired regions, but not so strong that it makes the contour move beyond the true cranial wall. We have found experimentally that  $\lambda = 0.15$  is a good general-purpose choice. We are currently investigating ways of adjusting  $\lambda$  automatically.

The structure of the algorithm used for the cranial cross sections is basically the same as the one developed for the femur. There are only three important differences:

- (1) The log-likelihood function being maximized is modified with the balloon term (Equation (8)).
- (2) The algorithm is divided into two phases: in a first phase, only control points  $[P_1, P_2, P_3, P_4]$  (see Figure 2) are considered (that is, the contour is a spline with four control points). After convergence, four more control points are inserted,  $[P_5, P_6, P_7, P_8]$  (see Figure 2) and the algorithm continues until it converges to a final estimate. The basic idea behind this approach is that during the first iterations, when the contour estimate is far from its final position, a coarse representation is sufficient and the algorithm proceeds much faster. In the final iterations, a finer adjustment of the shape is possible with the extra control points.
- (3) Initialization is performed as follows: the user indicates a point somewhere close to the center of the head; points  $P_1, P_2, P_3,$  and  $P_4$  are placed in such a way that the contour they define is a small ellipse around the given point.

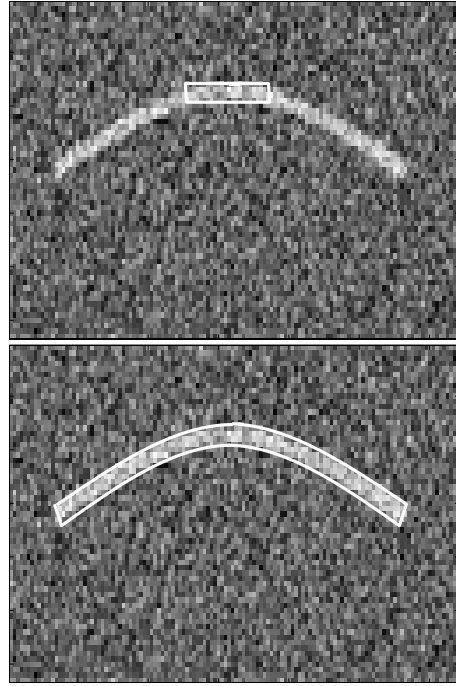


Figure 3 - Initial and final estimates on a synthetic image representing a femur.

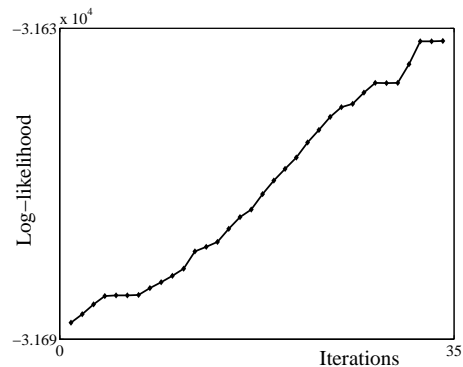


Figure 4 - Evolution of the log-likelihood for the example of Figure 3.

## V. EXPERIMENTS

### A. Synthetic Images

The first two examples simply illustrate the behavior of the algorithm using synthetic images generated according to the Rayleigh model. In Figure 3 we simulate a femur, with the inner and outer variances set to 156 and 116, respectively; the figure shows the initial contour and the final one obtained after 34 iterations. The evolution of the log-likelihood function is plotted in Figure 4. The image model parameter estimates obtained were  $\hat{\sigma}_{in} = 156.05$  and  $\hat{\sigma}_{out} = 115.70$ , very close to the true ones.

In the example of Figure 5, resembling a cranial cross-section, the inner and outer regions have variance 60.77 and 42.95, respectively. The log-likelihood evolution is plotted in Figure 6; the transition from the first to second stage of the algorithm occurred at iteration 22. The final parameter estimates are  $\sigma_{in} = 62.49$  and  $\sigma_{out} = 42.94$ , again very close to the true values.

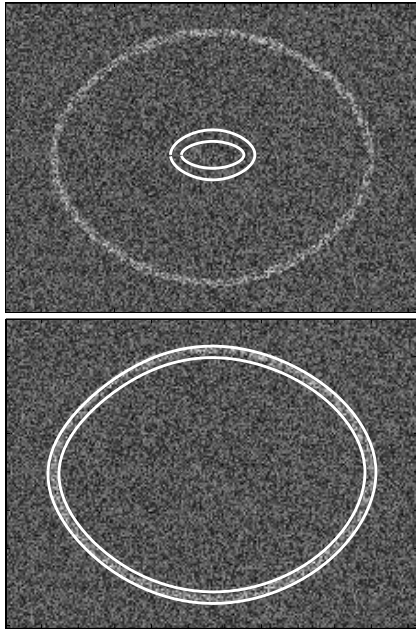


Figure 5 - Initial and final estimates on a synthetic image representing a cranial cross-section.

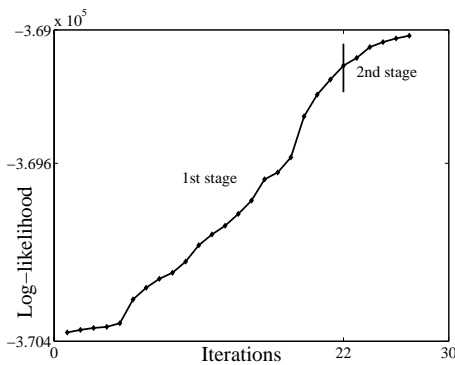


Figure 6 - Evolution of the log-likelihood for the example of Figure 5.

### B. Real images

Figures 7, 8, and 9 show examples of femur contour estimates on real echographic images. We recall that the only interaction required from the user is to indicate a point somewhere on the femur. No parameter adjustments are needed. These estimates were considered very good by expert clinicians.

Figures 10, 11, and 12 show examples of cranial cross-section contour estimates on real echographic images. We recall that the only interaction required from the user is to indicate a point somewhere close to the center of the head. The initial contour obtained by the algorithm, around the point given by the user, are shown as dashed lines. Again, we stress that no parameter adjustments are needed. These final contours were also considered very good by experts.

### C. Measurements

Figures 9 and 12 show the femur and cranial cross-section of a fetus, taken during an obstetric exam. The measurements obtained via the automatically estimated contours are FL = 3.09 cm (GA = 19 w 2 d) and BDP = 4.33 cm

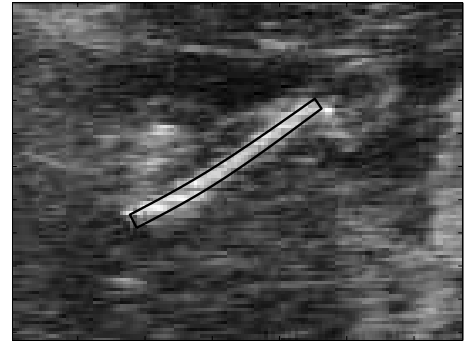


Figure 7 - Example of femur contour estimation on a real image.

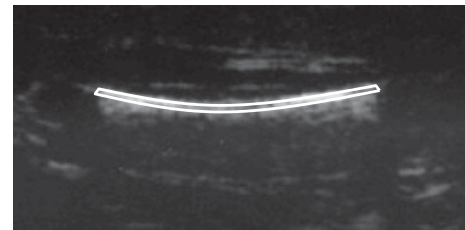


Figure 8 - Example of femur contour estimation on a real image.

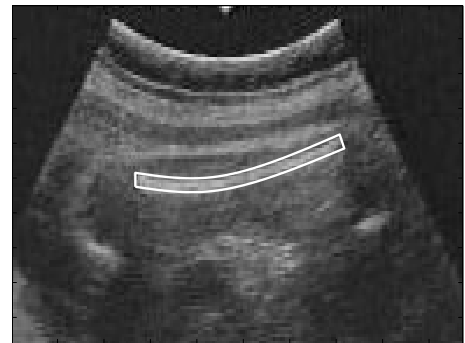


Figure 9 - Example of femur contour estimation on a real image.

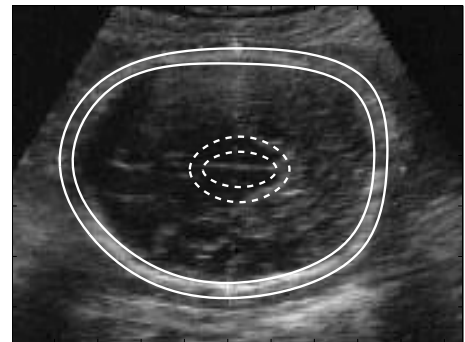


Figure 10 - Example of cranial cross-section contour estimation on a real image.

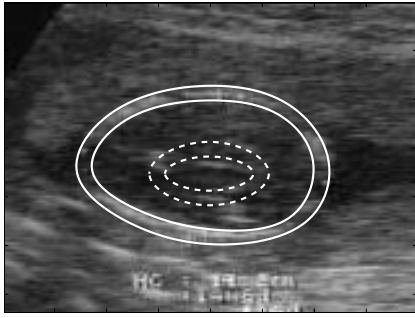


Figure 11 - Example of cranial cross-section contour estimation on a real image.

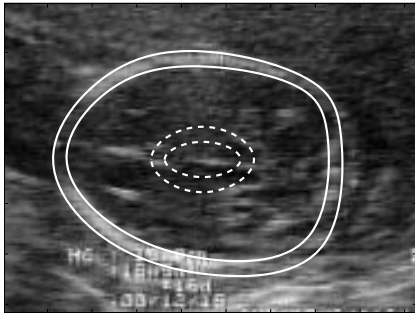


Figure 12 - Example of cranial cross-section contour estimation on a real image.

(GA = 19 w 1 d). Manual measurement gives FL = 3.0 cm (GA = 18 w 5 d) and BDP = 4.0 cm (GA = 19 w 0 d). For Figures 10 and 7, which also correspond to one fetus, the automatically obtained measurements are FL = 5.8 cm (GA = 30 w 1 d) and BDP = 7.42 cm (GA = 30 w 2 d); parameters values for manual extraction are FL = 6.1 cm (GA = 31 w 4 d) and BDP = 7.4 cm (GA = 30 w 0 d). We verify that in both examples the difference between gestational age obtained for FL and BPD parameters via the automatic contour extraction is 1 day, while for manual extraction is 2 days for the first example and 1 week and 4 days for the second. Although, of course, more experiments are needed, this seems to suggest a good consistency of the measurements obtained automatically.

## VI. CONCLUDING REMARKS

This paper described an approach to unsupervised contour estimation of fetal anatomic structures. All the model parameters are considered unknown and estimated from the observed image. Examples presented, using synthetic and real images, showed the ability of the proposed method to estimate contours in an unsupervised manner, i.e. adapting to a not completely known shape and observation parameters. With the synthetic images, the good match between the estimated and the true parameters also shows the good performance of the approach.

Future work will include a thorough experimental evaluation of consistency, robustness, and reproducibility.

## REFERENCES

[1] J. Duncan and N. Ayache, "Medical image analysis: Progress over two decades and the challenges ahead", *IEEE Transactions on Pat-*

- tern Analysis and Machine Intelligence*, vol. 22, pp. 85–106, 2000.
- [2] R. Sanders and A. James, *The Principles and Practice of Ultrasonography in Obstetrics and Gynecology*, Appleton-Century-Crofts, Connecticut, 1985.
- [3] C. W. Hanna and A. B. Youssef, "Automated measurements in obstetric ultrasound images", *Proceedings of the International Conference on Image Processing*, pp. 504–507, 1997.
- [4] J. Thomas, R. Peters II, and P. Jeanty, "Automatic segmentation of ultrasound images using morphological operators", *IEEE Transactions on Medical Imaging*, vol. 10, no. 2, pp. 180–186, 1991.
- [5] R. Powis and W. Powis, *A Thinker's Guide to Ultrasonic Imaging*, Urban And Schwartzberg Inc., 1984.
- [6] C. Burckhardt, "Speckle in ultrasound b-mode scans", *IEEE Transactions on Sonics and Ultrasonics*, vol. 25, pp. 1–6, 1978.
- [7] J. Dias and J. Leitão, "Wall position and thickness estimation from sequences of echocardiographic images", *IEEE Transactions on Medical Imaging*, vol. 15, no. 1, pp. 25–38, 1996.
- [8] M. Kass, A. Witkin, and D. Terzopoulos, "Snakes: Active contour models", *Proceedings of the First International Conference on Computer Vision*, pp. 259–268, 1987.
- [9] M. Figueiredo, J. Leitão, and A. K. Jain, "Unsupervised contour representation and estimation using B-splines and a minimum description length criterion", *IEEE Transactions on Image Processing*, vol. 9, pp. 1075–1087, 2000.
- [10] A. Chakrabarty, L. Staib, and J. Duncan, "Deformable boundary finding influenced by region homogeneity", *Proceedings of the IEEE Conference on Computer Vision and Pattern Recognition*, pp. 624–627, 1994.
- [11] L. Cohen, "On active contour models and balloons", *Computer Vision, Graphics, and Image Processing (CVGIP): Image Understanding*, vol. 53, no. 2, pp. 211–218, 1991.
- [12] M. Figueiredo and J. Leitão, "Bayesian estimation of ventricular contours in angiographic images", *IEEE Transactions on Medical Imaging*, vol. 11, no. 3, pp. 416–429, 1992.
- [13] T. McInerney and D. Terzopoulos, "Topologically adaptable snakes", *Proceedings of the IEEE International Conference on Computer Vision*, pp. 840–845, 1995.
- [14] R. Ronfard, "Region-based strategies for active contour models", *International Journal of Computer Vision*, vol. 13, pp. 229–251, 1994.
- [15] S. Zhu and A. Yuille, "Region competition: Unifying snakes, region growing, energy/Bayes/MDL for multi-band image segmentation", *IEEE Transactions on Pattern Analysis and Machine Intelligence*, vol. 18, pp. 884–900, 1996.
- [16] U. Grenander, *General Pattern Theory: A Mathematical Study of Regular Structures*, Oxford University Press, Oxford, 1993.
- [17] M. Figueiredo, J. Leitão, and A. K. Jain, "Adaptive parametrically deformable contours", in *Energy Minimization Methods in Computer Vision and Pattern Recognition*, M. Pellilo and E. Hancock, Eds. 1997, pp. 35–50, Springer Verlag.
- [18] A. K. Jain, Y. Zhong, and M. P. Dubuisson-Jolly, "Deformable template models: A review", *Signal Processing*, vol. 71, pp. 109–129, December 1998.
- [19] L. Staib and J. Duncan, "Boundary finding with parametrically deformable models", *IEEE Transactions on Pattern Analysis and Machine Intelligence*, vol. 14, no. 11, pp. 1061–1075, November 1992.
- [20] A. Yuille and P. Hallinan, "Deformable templates", in *Active Vision*, A. Blake and A. Yuille, Eds., pp. 21–38. MIT Press, 1992.